Faraday Discussions
Cite this: *Faraday Discuss.*, 2024, **249**, 440

PAPER

How do water-mediated interactions and osmotic second virial coefficients vary with particle size?

Hidefumi Naito, [ab] Tomonari Sumi [ab] and Kenichiro Koga *[ab]

Received 19th May 2023, Accepted 21st July 2023
DOI: 10.1039/d3fd00104k

We examine quantitatively the solute-size dependences of the effective interactions between nonpolar solutes in water and in a simple liquid. The potential $w(r)$ of mean force and the osmotic second virial coefficients B are calculated with high accuracy from molecular dynamics simulations. As the solute diameter increases from methane's to C_{60}'s with the solute–solute and solute–solvent attractive interaction parameters fixed to those for the methane–methane and methane–water interactions, the first minimum of $w(r)$ lowers from -1.1 to -4.7 in units of the thermal energy kT. Correspondingly, the magnitude of B (<0) increases proportional to σ^{α} with some power close to 6 or 7, which reinforces the solute-size dependence of B found earlier for a smaller range of σ [H. Naito, R. Okamoto, T. Sumi and K. Koga, *J. Chem. Phys.*, 2022, **156**, 221104]. We also demonstrate that the strength of the attractive interactions between solute and solvent molecules can qualitatively change the characteristics of the effective pair interaction between solute particles, both in water and in a simple liquid. If the solute–solvent attractive force is set to be weaker (stronger) than a threshold, the effective interaction becomes increasingly attractive (repulsive) with increasing solute size.

1 Introduction

We report here the results of computer simulation studies on the effective pair interactions between spherical solute particles with varying diameters in water and in a simple liquid.

When a hydrophobic molecule is transferred into water from a gas phase or from an oily phase, the change in enthalpy is negative but the change in solvation entropy (the relevant part of the change in entropy) is also negative, and the entropic contribution is greater than the enthalpic one, leading to the positive solvation free energy (change) and the low solubility of the hydrophobe in water.

[a]*Department of Chemistry, Faculty of Science, Okayama University, Okayama 700-8530, Japan. E-mail: koga@okayama-u.ac.jp*
[b]*Research Institute for Interdisciplinary Science, Okayama University, Okayama 700-8530, Japan*

This is the basic mechanism characteristic of the hydrophobic hydration.[1–3] When two such hydrophobic solute molecules are in contact with each other in water, the solvation free energy for the pair is less than that for two molecules far apart, resulting in water-mediated attraction between them, the hydrophobic attraction.[2,3]

The solvent-mediated pair interaction between solute molecules in a solvent is fully described by the potential $w(r)$ of mean force, which is the sum of the direct pair potential $\phi(r)$ and the solvent-induced part $w^*(r)$. The strength of that interaction may be measured by the first minimum of $w(r)$, or equivalently the first peak of the radial distribution function $g(r) = \mathrm{e}^{-w(r)/kT}$, and the osmotic second virial coefficient B. The osmotic B, the second coefficient of the expansion of the osmotic pressure in the solute density ρ at fixed chemical potentials of solvent species and fixed temperature, is given by the correlation-function integral:[4]

$$B = -\frac{1}{2}\lim_{\rho\to 0}\int\left[g(r)-1\right]\mathrm{d}\tau = -\frac{1}{2}G, \tag{1}$$

where $\mathrm{d}\tau$ is an infinitesimal volume element and G is the solute–solute Kirkwood–Buff (KB) integral[5] at infinite dilution. Experimental data for B are sparse compared to solubility data, and so molecular simulation and theory of liquids are indispensable tools for evaluating B.[6–18]

It has been recognized in physical chemistry and biochemistry that the size of solute molecules (inert gases, hydrocarbons, amphiphiles, proteins, and so on) matters to the hydration free energy and the hydrophobic interaction. The subject has been extensively discussed in the literature.[19–42] In a wider framework, the solute-size effect on the effective pair potential $w(r)$ in simple liquids has been an important subject in the theory of liquids.[43–49]

The present paper aims at a quantitative understanding of how the strength of effective pair interaction between solute molecules in water, changes with solute size. Recently it was reported[15] that the osmotic second virial coefficient B for Lennard-Jones (LJ) particles in water varies with diameter σ as $\sim\sigma^{\alpha}$ with $\alpha \simeq 6$ in the range $\sigma \leq 2\sigma_{\mathrm{m}}$, where σ_{m} is the LJ diameter of methane. The change in B in that range is already enormous because of the large power. Now we extend the upper limit of σ to $3\sigma_{\mathrm{m}} \simeq 1.12$ nm, which then covers solutes ranging from methane to C_{60}, and examine whether or not the power-law dependence continues to hold. The second issue addressed in the present paper is the effect of the solute–solvent attractive interaction on the solute-size dependences of $w(r)$ and B. At ambient conditions the solvent-mediated interactions between hydrophobic molecules, between amphiphilic molecules, and between hydrophobic groups in proteins in aqueous solution are less attractive than the direct interactions due to the existence of the solute–solvent attractive interactions.[7,10,14,50,51] To be specific, take the case of methane in water, as an example: the osmotic B for methane and the gas virial coefficient B_{gas} are both negative at ambient temperatures, but more importantly $B > B_{\mathrm{gas}}$, *i.e.*, methane particles are less attractive in water than in vacuum. The difference between B and B_{gas} becomes greater at lower temperatures.[7,10] On the other hand, hard-sphere solutes are more attractive in water than in vacuum as $B < 0$ and $B_{\mathrm{gas}} > 0$.[9] Thus, the attractive forces between solute and solvent molecules is a key factor that could change the characteristics of the effective interaction between solute molecules.

In the present study we calculate $w(r)$ and B for solute species with different diameters and different strengths of the solute–solvent attraction in order to gain a quantitative understanding of the effect of the solute–solvent attraction on the solute-size dependence of $w(r)$ and B. The next important question to be addressed is what kinds of features in the solute-size dependence of the hydrophobic interaction are universal for liquid mixtures in general and what is unique for water. As a first step, we evaluate the solute size dependences of $w(r)$ and B for LJ mixtures and compare the results with those for water.

2 Computational details

We examine the model systems for aqueous solutions of hydrophobic solutes and, for comparison, those for simple liquid mixtures. Molecular dynamics (MD) simulations are performed for aqueous and non-aqueous solutions to obtain the effective pair potential between solute molecules.

The systems for aqueous solutions consist of water molecules interacting with each other *via* the TIP4P/2005 potential[52] and spherical solute particles interacting with each other *via* the LJ potential:

$$\phi(r) = 4\varepsilon\left[\left(\frac{\sigma}{r}\right)^{12} - \left(\frac{\sigma}{r}\right)^{6}\right]. \tag{2}$$

Note that ε is fixed when evaluating the effective solute–solute interactions as a function of the solute diameter σ. The solute–water pair interactions are modeled by the LJ potential $\phi_{uv}^{LJ}(r)$ or the repulsive Weeks–Anderson–Chandler (WCA) potential,

$$\phi_{uv}^{WCA}(r) = \begin{cases} \phi_{uv}^{LJ}(r) + \varepsilon_{uv} & \left(r < 2^{1/6}\sigma_{uv}\right) \\ 0 & (\text{otherwise}) \end{cases}. \tag{3}$$

The reference hydrophobic solute is taken to be methane modeled by the TraPPE-UA force field,[53] whose LJ parameters are $\sigma_m = 0.373$ nm and $\varepsilon_m = 1.23$ kJ mol^{-1}. The solute particles with different diameters are those with $\sigma^* = \sigma/\sigma_m = 1$, 1.5, 2, 2.5, and 3, and $\varepsilon = \varepsilon_m$. Recently the σ dependences of the solute–solute radial distribution function $g(r)$ and the osmotic second virial coefficient B have been reported for the LJ solutes with $\sigma^* \leq 2$.[15] For the solute–water LJ pair interactions, the size parameter σ_{uv} is set to $\sigma_{uv} = (\sigma + \sigma_w)/2$ with σ_w of the TIP4P/2005 water. The energy parameter $\varepsilon_{uv}^* = \varepsilon_{uv}/\varepsilon_0$ is fixed to either 1, 2, or 3, where $\varepsilon_0 = 0.977$ kJ mol^{-1}, the value given by $\sqrt{\varepsilon_m \varepsilon_w}$ with ε_w of the TIP4P/2005 model water.

The number N_v of water molecules and the number N of solute particles depend on the model system, as listed in Table 1. For the systems with $N = 20$, 40, and 80, standard MD simulations were performed to obtain $g(r)$; for those with $N = 2$, the umbrella sampling method[54,55] was applied.

We performed isobaric–isothermal MD simulations for the model aqueous solutions under three-dimensional periodic boundary conditions using GROMACS 2018.[56] The pressure is set to 1 bar using the Parrinello–Rahman method and the temperature is maintained at 300 K by the Nosé–Hoover method. For the systems with $N = 20$ and above, the duration time t of the production run is 100

Table 1 Model systems: solvent and solute species, solute diameter σ^*, the solute–solvent LJ energy parameter ε^*_{uv} (for WCA solutes this is the parameter in eqn (3)), and numbers N_v and N of solvent and solute molecules, respectively. The solute–solute potential is of the LJ form for all systems.

Solvent	Solute–solvent potential function	σ^*	ε^*_{uv}	N_v	N
Water	LJ	1	1	4000	40
	LJ	1	2, 3	4000	20
	LJ	1.5	1	4000	20
	LJ	2	1	8000	2
	LJ	2	2, 3	8000	40
	LJ	2.5, 3	1	8000	2
	LJ	3	2, 3	16 000	80
	WCA	1	1	4000	2
	WCA	2, 3	1	8000	2
LJ	LJ	1	0.5, 1, 2	5000	20
	LJ	2	0.5, 1, 2	10 000	20
	LJ	3	0.5, 1, 2	20 000	40

ns, except for the system with the solute particles of diameter $\sigma^* = 1.5$, in which case $t = 200$ ns. In the umbrella sampling method, t for each simulation with a given constraint for the distance between two solute particles is 20 ns except for the system with the WCA solute particles of $\sigma^* = 1$, in which case $t = 10$ ns. The time step interval of each simulation is 1 fs. The configurations of solute molecules were recorded every 0.05 ps to compute $g(r)$.

In the umbrella sampling simulations, the harmonic potential with the spring constant of 1000 kJ mol^{-1} nm^{-2} was applied to constrain the distance between the two solute particles. The constraint distance ranges from 0.6 to 2.9 nm for $\sigma^* = 2$ and from 0.7 to 2.8 nm for $\sigma^* = 2.5$, and from 0.8 to 3.1 nm for $\sigma^* = 3$, in 0.1 nm increments. For the WCA solutes, *i.e.*, those which interact with solvent molecules *via* the WCA pair potential $\phi^{WCA}_{uv}(r)$, the constraint distance ranges from 0.2 to 2.5 nm for $\sigma^* = 1$ and from 0.6 to 2.9 nm for $\sigma^* = 2$, and from 0.8 to 3.1 nm for $\sigma^* = 3$. The potentials $w(r)$ of mean force were obtained from the weighted histogram analysis method.[57,58]

All the LJ pair potentials in each model aqueous solution were truncated at a cutoff distance r_{cut}, its value depending on the solute size σ^*: $r_{cut} = 1.3$ nm for $\sigma^* = 1$ and 1.5, $r_{cut} = 2$ nm for $\sigma^* = 2$ and 2.5, and $r_{cut} = 2.4$ nm for $\sigma^* = 3$. The Coulomb potentials were treated using the particle mesh Ewald method with the cutoff distances in the real space being the same as r_{cut} of the LJ potentials.

In order to calculate $g(r)$, or equivalently $w(r)$, for hydrophobic solutes at infinite dilution from MD simulations for the model solutions at finite concentration, we employed the following technique when necessary. When performing MD simulations for the systems containing solute particles ($N = 40$ or 20, $N_v = 4000$) with $\sigma^* = 1$ or 1.5 and $\varepsilon^*_{uv} = 1$, the LJ potential for the solute–solute interactions was replaced by a repulsive potential $\phi^{rep}(r)$, and then the resulting radial distribution function $g_{rep}(r)$ was converted to $g(r)$ by the identity $g(r) = \lim_{\rho \to 0} g_{rep}(r) \exp[-\phi^{att}(r)/kT]$ with $\phi^{att}(r) = \phi^{LJ}(r) - \phi^{rep}(r)$. Here we assume that $g_{rep}(r)$ obtained from the simulation is very close to that at infinite dilution because the solute particles have no tendency of aggregation due to the potential $\phi^{rep}(r)$. For

the solute with $\sigma^* = 1$, $\phi^{\mathrm{rep}}(r)$ is the repulsive WCA potential, the solute–solute analog of eqn (3), while for the solute with $\sigma^* = 1.5$, $\phi^{\mathrm{rep}}(r)$ is $4\varepsilon(\sigma/r)^{12}$.

We also studied models of nonpolar solutions (simple liquid mixtures) to compare the solute-size dependences of $w(r)$ and B with those in the aqueous solutions. The systems consist of two components of LJ particles. All quantities such as the distance, the solvent density, and temperature, are given in reduced units of the LJ parameters σ_{v} and ε_{v} of solvent particles. We consider solutes with $\sigma^*(=\sigma/\sigma_{\mathrm{v}}) = 1$, 2, 3 and $\varepsilon^*(=\varepsilon/\varepsilon_{\mathrm{v}}) = 1$. The solute–solvent LJ potential parameters are set to $\sigma^*_{\mathrm{uv}} = (\sigma^* + 1)/2$ and $\varepsilon^*_{\mathrm{uv}} = 0.5,\ 1,\ 2$. The solvent number density and the temperature are set to $\rho^*_{\mathrm{v}}(= \rho_{\mathrm{v}}\sigma_{\mathrm{v}}^3) = 0.8$ and $T^*(=kT/\varepsilon_{\mathrm{v}}) = 1.5$. This density ρ^*_{v}, is close to 0.85, the density of the LJ liquid at the triple point, and the temperature T^* is higher than the critical point.[59] At this state point, Kimura and Yoshimura calculated $g(r)$ for the solutes with $\sigma^* = 0.5$, 1, 1.5, $\varepsilon^* = 1$, and $\varepsilon^*_{\mathrm{uv}} = 1,\ 2$ using the integral equation theory.[60]

We performed isochoric–isothermal MD simulations of the LJ mixtures. The numbers of solvent and solute particles are given in Table 1. The duration time t^* of the production run and the cutoff distance r^*_{cut} of the LJ potential depend on the system: for the systems with $\sigma^* = 1$, $t^* = 84\,659$ and $r^*_{\mathrm{cut}} = 3.077$; for $\sigma^* = 2$ and 3, $t^* = 169\,318$ and $r^*_{\mathrm{cut}} = 6.154$. In the case of $\sigma^* = 3$, the solute–solute LJ potential was replaced by the repulsive WCA potential and the resulting radial distribution function was converted to $g(r)$ as in the cases of the model aqueous solutions.

When one calculates B from eqn (1) using numerical integration, one finds large errors or even diverging behavior of the integral. This is because $g(r)$ obtained for a closed system does not converge to 1, because statistical errors in $g(r)$ at large distances are enhanced by the factor r^2, and because there is the finite-size effect in any simulation. To overcome this problem, we employed the method described in our previous paper.[7,15] First, we correct the limiting behavior of $g(r)$ so that the average of $g(r)$ over a certain range at long distances becomes 1. Second, we use the method proposed by Krüger *et al.*[61,62] for evaluating the KB integral at the thermodynamic limit from that of the finite systems:

$$G(L) = \int_0^L [g(r) - 1]4\pi r^2 \left[1 - \frac{3}{2}\left(\frac{r}{L}\right) + \frac{1}{2}\left(\frac{r}{L}\right)^3\right] \mathrm{d}r, \tag{4}$$

$$G(L)L = GL + C. \tag{5}$$

where L is the upper limit of the integral and C is a constant. From eqn (4) with corrected $g(r)$, one obtains $G(L)$ as a function of L. One then plots $G(L)L$ against L and finds a certain range of L where the linear relation, eqn (5), holds. The linear fit to the data in that range of L gives the KB integral G.

3 Results and discussion

First, we examine how the hydrophobic interaction (the effective pair potential between nonpolar solute particles in water) changes when the solute size increases while nothing else changes. Fig. 1(a) displays the radial distribution functions $g(r)$ for pairs of LJ particles in water, each corresponding to the solute with a different diameter σ but the same energy parameters $\varepsilon = \varepsilon_{\mathrm{m}}$ and $\varepsilon_{\mathrm{uv}} = \varepsilon_0$. It

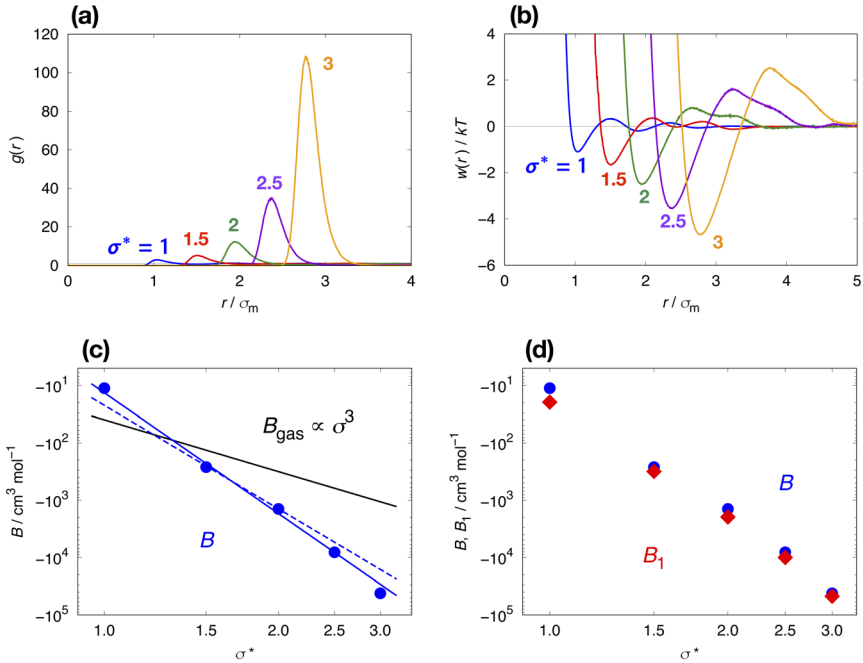

Fig. 1 (a) The radial distribution functions $g(r)$ for LJ particles of different sizes in water. The LJ solute diameters are $\sigma^*(=\sigma/\sigma_m) = 1$, 1.5, 2, 2.5, and 3, with $\sigma_m = 0.373$ nm; the LJ energy parameters are fixed to $\varepsilon = \varepsilon_m = 1.23$ kJ mol^{-1}. (b) The corresponding potentials $w(r)$ of mean force. (c) The log–log plots of the osmotic second virial coefficients B against σ^*. The best fits of the 6th (dotted blue line) and 7th (solid blue line) power law and the second virial coefficient B_{gas} for the LJ gas, which follows the cubic power law, are also plotted. (d) The log–log plots of B *vs.* σ^* and $B_1 = -2\pi \int_0^{r_1} [\exp[-w(r)/kT] - 1] r^2 dr$ *vs.* σ^* with r_1 the distance of the first maximum of $w(r)$.

is clear that the first peak develops rapidly with increasing particle diameter σ. The corresponding potentials $w(r)$ of mean force are shown in Fig. 1(b). The potential well depth becomes deeper as σ increases: $w(r)/kT$ at the first minimum is −1.10, −1.66, − 2.50, −3.56, and −4.69 at $\sigma^* = 1$, 1.5, 2, 2.5, and 3, respectively.

The variation of $w(r)/kT$ at the first minimum with increasing solute size is essentially due to changes in the solvent-induced part of the effective interaction since the solute–solute LJ parameter ε is fixed. In general, solvent-induced attraction at the solute–solute contact distance is largely due to the excluded volume effect. Each particle has an excluded volume from which solvent molecules or co-solvent molecules are excluded. When the two particles are held fixed at some short distance, the two excluded-volume spheres overlap, and the larger the overlapping volume (*e.g.*, the shorter the inter-particle distance) the greater the configurational entropy of solvent (or co-solvent) molecules and thus the lower the solvation free energy of the pair of particles.[63,64] When the Asakura–Oosawa (AO) theory[65] is applied to a hard-sphere fluid consisting of solvent and solute particles, the effective pair potential at contact distance σ, which is the minimum in the AO potential $w^{AO}(r)$, decreases linearly with σ, the diameter of the solute particles:

$$\frac{w^{\mathrm{AO}}(\sigma)}{\eta kT} = -\frac{3}{2}\sigma - 1, \tag{6}$$

where σ is now in units of diameter of the solvent particles and η is the packing fraction of the solvent. Thus the effective potential at the first minimum for the hydrophobic particles in water (Fig. 1(b)) and the AO potential at contact distance (eqn (6)) have the same trend in terms of solute-size dependence. However, the magnitude of the solvent-induced interaction is much stronger in the hydrophobic interactions than in the AO potential and the solute-size dependence of $w(r)$ at the first minimum is stronger than the linear dependence.

Apart from the size dependence of the first minimum of $w(r)$, Fig. 1(b) also indicates that both the first maximum and the second minimum of $w(r)$ move up with increasing σ, and the second minimum disappears at $\sigma^* = 2$. This trend may well be characteristic of the hydrophobic interaction. Earlier studies showed that the force curve between hydrophobic planar sheets in water becomes increasingly repulsive as the two sheets approach each other and squeeze bilayer water.[66,67] It is possible that the force curve between hydrophobic particles with $\sigma^* = 3$ already bears a strong resemblance to that between hydrophobic surfaces. However, the correspondence is a matter of conjecture and further analysis is needed.

Fig. 1(c) is the log–log plot of the osmotic second virial coefficients B against σ^*. The values of B are negative for all solutes with different σ, *i.e.*, their effective interactions in water are attractive. The magnitude of B becomes larger with increasing σ. The dotted and solid lines indicate linear fits to the data with slopes of 6 and 7, respectively. The log–log plot of B *vs.* σ^* seems to follow a linear relationship, *i.e.*,

$$B \propto \sigma^{*\alpha}. \tag{7}$$

The best estimate of α is close to 7 and in between 6 and 7 for the range of $\sigma^* \leq 3$. In ref. 15, it was conjectured that $B \propto \sigma^{*6}$ for a smaller range of σ^* ($\sigma^* \leq 2$) and it was remarked that the 6th power law accords with the thermodynamic identity:[68,69]

$$B = B'' - \frac{v^{*2}}{2kT\chi}, \tag{8}$$

where B'' is an analog of B, the coefficient of ρ^2 in the ρ expansion of the osmotic pressure at fixed density of the solvent (not at fixed chemical potential of the solvent); v^* is the solvation molecular volume of the solute at infinite dilution and χ is the isothermal compressibility of pure solvent. The second term in eqn (8) is proportional to σ^{*6}. However, we note that eqn (8) provides the lower bound of the size dependence of B, because the size dependence of B'' could be stronger than the second term, and thus the present result is not inconsistent with the thermodynamic identity. Note that the second virial coefficient B_{gas} for the LJ gas (*i.e.*, without any solvent) is strictly proportional to σ^3 at fixed ε as shown in Fig. 1(c). It is the solvent-induced attraction that causes the much greater solute-size dependence of B (eqn (7)) compared with that of B_{gas}.

The potential of mean force $w(r)$ between two solute particles or the corresponding pair correlation function $g(r) - 1$ is not a simple function of r and exhibits damped oscillatory decay, in contrast to the pair potential $\phi(r)$ in eqn (2)

or $e^{-\phi(r)/kT} - 1$, which decays monotonically. Thus it is worth examining which range of r contributes primarily to the σ dependence of B. Let B_1 be the contribution to B from $w(r)$ in the short range $r < r_1$, where r_1 is the distance of the first maximum of $w(r)$: $B_1 = -\frac{1}{2}\int_{r<r_1} [g(r) - 1]d\tau$. Comparing the log–log plot of B_1 with that of B (Fig. 1(d)), we find that the dominant contribution to the solute-size dependence of B comes from the short range of r.

Next, we examine the effect of the solute–solvent attractive interaction on the effective pair potential $w(r)$ between solute particles in water. For solutes with a given σ^*, three different solute–solvent LJ potentials are considered: $\varepsilon^*_{uv}(= \varepsilon_{uv}/\varepsilon_0) = 1,\ 2,$ and 3. In addition, the repulsive WCA potential is also assumed for the solute–solvent interaction. For each case of $\sigma^* = 1$, 2 and 3, as shown in Fig. 2(a)–(c), respectively, the potential curve of $w(r)$ over a short range, including its first minimum and the first maximum, shifts upwards as the solute–solvent attraction is strengthened by increasing ε^*_{uv} from 1 to 3. When the solute–solvent interaction is purely repulsive, *i.e.*, when it is the repulsive WCA potential, the potential of mean force in the same range is well below that for the reference LJ potential ($\varepsilon^*_{uv} = 1$). The results described above are in accord with the observations that the solvent-induced part of $w(r)$ is weakened by the solute–solvent attractive interactions[12,29,31,35–37,70–74] and that in some cases the hydrophobic

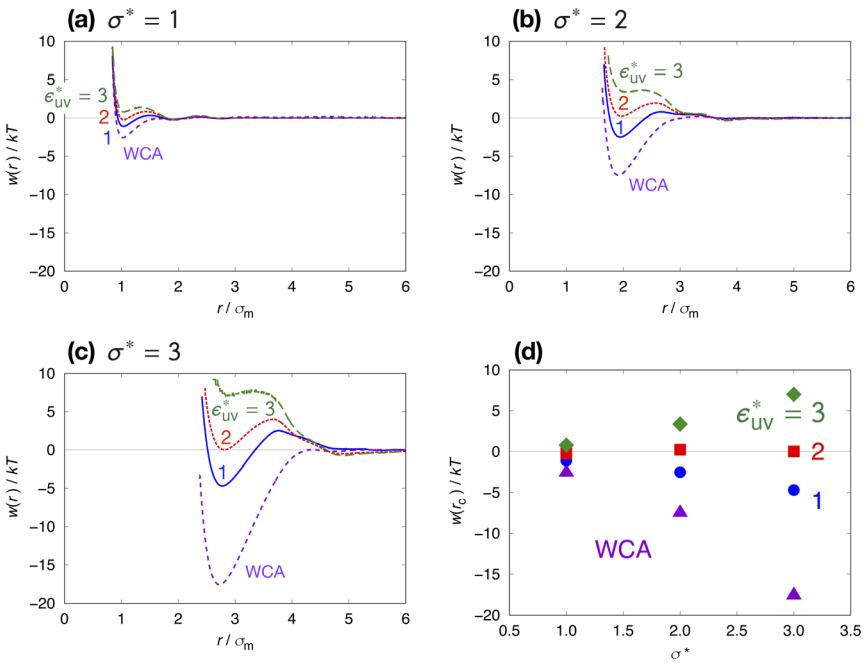

Fig. 2 Effects of the solute–solvent attractive interaction on $w(r)$ for LJ solutes in water at 1 bar and 300 K. The solute diameter is fixed at (a) $\sigma^* = 1$, (b) $\sigma^* = 2$, and (c) $\sigma^* = 3$. Dashed "WCA" curves mark the repulsive WCA potential, and solid, dotted and long dashed curves are the $w(r)$ for solutes interacting with water *via* the LJ potential with $\varepsilon^*_{uv} = 1,\ 2,$ and 3, respectively. (d) The first minimum $w(r_c)$ of $w(r)$ as a function of σ^* for the four different solute–solvent pair potentials.

interactions between nonpolar molecules in water are not as attractive as those in other environments.[50,51,74]

Comparing Fig. 2(a), (b) and (c), it is clear that the effect of the solute–solvent attractive interaction is greater for larger solute particles. To quantify this tendency, we focus on the first minimum in $w(r)$, *i.e.*, $w(r_c)$ with r_c being the distance of the first minimum, which depends on σ and ε_{uv}. Note that r_c is close to σ, the solute–solute contact distance, but is slightly smaller. The plots of $w(r_c)/kT$ as a function of σ^* are shown in Fig. 2(d). Our reference set of solutes is the one with $\varepsilon^*_{uv} = 1$, *i.e.*, $\varepsilon_{uv} = 0.977$ kJ mol^{-1}, which corresponds to the dispersion force between methane and water molecules. When the solute–solvent attractive interaction is completely turned off (the repulsive WCA potential), $w(r_c)$ for a given σ^* becomes more negative than that for the reference set and the rate of change of $w(r_c)$ with σ^* is much greater than that for the reference set. On the other hand, when ε_{uv} is three times greater than that for the methane–water dispersion force, $w(r_c)$ is positive for any σ^* and increases with increasing σ^*. Thus, depending on the strength of solute–solvent attraction being smaller or greater than a certain threshold, the effective pair interaction becomes increasingly attractive or increasingly repulsive with the solute size, respectively. The threshold seems to be around $\varepsilon^*_{uv} = 2$ because then $w(r_c)/kT$ is close to 0 for any $\sigma^* \leq 3$.

We have seen how the effective pair interactions in water vary with solute size. Now we examine the solute-size dependence in a simple liquid using LJ mixtures. Fig. 3 shows the solute-size dependences of $g(r)$, $w(r)$, and B for three fixed values of the solute–solvent LJ energy parameter: $\varepsilon^*_{uv}(= \varepsilon_{uv}/\varepsilon_v) = 0.5,\ 1,$ and 2. For $\varepsilon^*_{uv} = 0.5$, as $\sigma^*(=\sigma/\sigma_v)$ increases the first peak of $g(r)$ develops, the first minimum of $w(r)$ decreases, and B decreases. These results are analogous to those for LJ solutes with $\varepsilon^*_{uv} = 1$ and the WCA solutes in water. We note that as σ^* increases the first maximum of $w(r)$ in the LJ solvent does not develop and the second minimum remains. This is a notable difference from what we observed for $w(r)$ in water. When ε^*_{uv} is fixed to 1, the size dependences of $g(r)$, $w(r)$, and B all show the opposite trends to those for $\varepsilon^*_{uv} = 0.5$, respectively. And when $\varepsilon^*_{uv} = 2$, solute particles of size $\sigma^* = 1$ in the solvent are barely attractive to each other: $w(r)$ at the first minimum is near zero and B is positive, and as σ^* increases, the effective interaction becomes increasingly repulsive. The threshold for ε^*_{uv} at which the solute-size dependence of $w(r)$ changes its character is between 0.5 and 1.

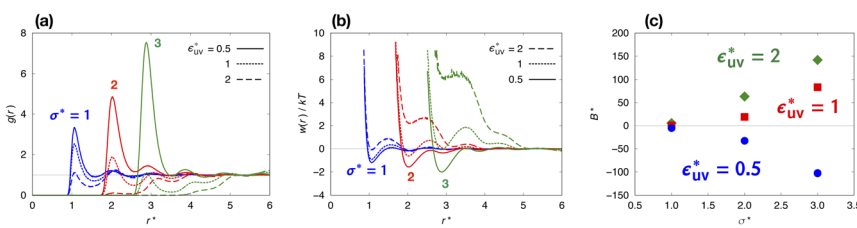

Fig. 3 The effective pair interactions between LJ solutes in the LJ solvent. (a) $g(r)$, (b) $w(r)/kT$, and (c) $B^*(=B/\sigma_v^3)$ for solutes with $\sigma^* = 1$, 2, 3, $\varepsilon^* = 1$, and $\varepsilon^*_{uv} = 0.5,\ 1,\ 2$. The state point of the LJ solvent is at $\rho^*_v = 0.8$, $T^* = 1.5$. Solid, dotted, and dashed curves are the results for $\varepsilon^*_{uv} = 0.5,\ 1,\ 2$, respectively.

4 Conclusions

To understand the hydrophobic interactions between solutes with varying sizes and varying solute–solvent interactions, we calculated and analyzed the effective pair interactions between nonpolar solutes in water, and for comparison, those in a simple liquid. The potentials $w(r)$ of mean force and the osmotic second virial coefficients B, were obtained with high accuracy based on MD simulations, so that their solute-size dependences could be considered quantitatively.

For the hydrophobic particles in water – whose solute–solvent LJ energy parameter ε_{uv} is fixed to be that of the methane–water pair – as the particle diameter σ increases, the effective pair potential $w(r_c)$ at contact distance decreases rapidly compared to the AO potential (eqn (6)), and at the same time the potential barrier following the first minimum becomes higher (Fig. 1(b)). Reflecting on such changes in $w(r)$, B becomes increasingly negative with increasing solute diameter as described by eqn (7). The power-law behavior of B *vs.* σ has been reported earlier[15] and here it is confirmed for a wider range of σ, from methane's to C_{60}'s.

The solute–solvent attractive interaction has a great influence on $w(r)$ (Fig. 2). With the solute–water pair, interaction is purely repulsive as given by the repulsive WCA potential, where $w(r_c)$ decreases most rapidly with σ. On the other hand, if the solute–water attractive interaction is sufficiently strong (*e.g.*, $\varepsilon^*_{uv} = 3$), $w(r_c)$ increases with σ. The threshold value of ε^*_{uv} at which the solute-size dependence of $w(r_c)$ changes qualitatively is found to be $\varepsilon^*_{uv} \simeq 2$. The effect of ε^*_{uv} on $w(r_c)$ for the solutes in a LJ solvent is qualitatively the same as that in water. It is anticipated that the solute size dependence of the osmotic B also changes qualitatively with the strength of solute–solvent attractive interaction.

Qualitatively, the results summarized above could be understood as follows. The main driving force for the effective pair interaction being increasingly attractive with increasing σ is the configurational entropy of solvent molecules (the excluded volume effect). However, the solute–solvent attractive interaction has an opposing effect since the potential energy due to the interactions of a pair of solute particles with surrounding solvent molecules is lower when the two particles are far from each other than when they are in contact. Therefore, when the solute–solvent attractive interaction is sufficiently strong, the effective pair interaction could be increasingly repulsive with increasing σ.

The solute-size dependence of the effective interaction is an important subject in the theory of liquids[43–49] and is also relevant to stability and phase separation in real systems such as colloidal solutions[75] and aqueous solutions in biological systems.[76,77] To understand more rigorously how the potential $w(r)$ of mean force and the osmotic B change with the solute size and how the solute–solvent attractive interaction alters the behaviors of $w(r)$ and B, both simulation-based and theoretical approaches which can examine a wider range of solute sizes are needed.

Conflicts of interest

There are no conflicts to declare.

Acknowledgements

This work was supported by KAKENHI (Grant Numbers 18KK0151 and 20H02696) and JST, the establishment of university fellowships towards the creations of science technology innovation (Grant Number JPMJFS2128). Part of the computation was performed at the Research Center for Computational Science, Okazaki, Japan (Project: 21-IMS-C125, 22-IMS-C124, 23-IMS-C112).

References

1 C. Tanford, *The Hydrophobic Effect: Formation of Micelles and Biological Membranes*, Wiley, New York, 2nd edn, 1980.
2 A. Ben-Naim, *Hydrophobic Interactions*, Plenum, Oxford, 1980.
3 B. Widom, P. Bhimalapuram and K. Koga, *Phys. Chem. Chem. Phys.*, 2003, **5**, 3085–3093.
4 W. G. McMillan Jr and J. E. Mayer, *J. Chem. Phys.*, 1945, **13**, 276–305.
5 J. G. Kirkwood and F. P. Buff, *J. Chem. Phys.*, 1951, **19**, 774–777.
6 L. R. Pratt and D. Chandler, *J. Solution Chem.*, 1980, **9**, 1–17.
7 K. Koga, *J. Phys. Chem. B*, 2013, **117**, 12619–12624.
8 K. Koga and B. Widom, *J. Chem. Phys.*, 2013, **138**, 114504.
9 M. I. Chaudhari, S. A. Holleran, H. S. Ashbaugh and L. R. Pratt, *Proc. Natl. Acad. Sci. U. S. A.*, 2013, **110**, 20557–20562.
10 H. S. Ashbaugh, K. Weiss, S. M. Williams, B. Meng and L. N. Surampudi, *J. Phys. Chem. B*, 2015, **119**, 6280–6294.
11 M. I. Chaudhari, D. Sabo, L. R. Pratt and S. B. Rempe, *J. Phys. Chem. B*, 2015, **119**, 9098–9102.
12 M. I. Chaudhari, S. B. Rempe, D. Asthagiri, L. Tan and L. Pratt, *J. Phys. Chem. B*, 2016, **120**, 1864–1870.
13 D. Tang, C. Delpo, O. Blackmon and H. S. Ashbaugh, *J. Chem. Phys.*, 2018, **148**, 016101.
14 K. Koga and N. Yamamoto, *J. Phys. Chem. B*, 2018, **122**, 3655–3665.
15 H. Naito, R. Okamoto, T. Sumi and K. Koga, *J. Chem. Phys.*, 2022, **156**, 221104.
16 C. A. Cerdeiriña and B. Widom, *J. Phys. Chem. B*, 2016, **120**, 13144–13151.
17 R. Okamoto and A. Onuki, *J. Chem. Phys.*, 2018, **149**, 014501.
18 R. Okamoto and K. Koga, *J. Phys. Chem. B*, 2021, **125**, 12820–12831.
19 G. Hummer, S. Garde, A. E. Garcia, A. Pohorille and L. R. Pratt, *Proc. Natl. Acad. Sci. U. S. A.*, 1996, **93**, 8951–8955.
20 G. Hummer and S. Garde, *Phys. Rev. Lett.*, 1998, **80**, 4193.
21 G. Graziano, *J. Chem. Soc., Faraday Trans.*, 1998, **94**, 3345–3352.
22 K. Lum, D. Chandler and J. D. Weeks, *J. Phys. Chem. B*, 1999, **103**, 4570–4577.
23 D. M. Huang, P. L. Geissler and D. Chandler, *J. Phys. Chem. B*, 2001, **105**, 6704–6709.
24 D. M. Huang and D. Chandler, *J. Phys. Chem. B*, 2002, **106**, 2047–2053.
25 N. T. Southall, K. A. Dill and A. Haymet, *J. Phys. Chem. B*, 2002, **106**, 521–533.
26 D. Chandler, *Nature*, 2005, **437**, 640–647.
27 S. Rajamani, T. M. Truskett and S. Garde, *Proc. Natl. Acad. Sci. U. S. A.*, 2005, **102**, 9475–9480.
28 H. S. Ashbaugh and L. R. Pratt, *Rev. Mod. Phys.*, 2006, **78**, 159.

29 E. Sobolewski, M. Makowski, C. Czaplewski, A. Liwo, S. Ołdziej and H. A. Scheraga, *J. Phys. Chem. B*, 2007, **111**, 10765–10774.
30 G. Graziano, *J. Phys. Chem. B*, 2009, **113**, 11232–11239.
31 M. Makowski, C. Czaplewski, A. Liwo and H. A. Scheraga, *J. Phys. Chem. B*, 2010, **114**, 993–1003.
32 R. Zangi, *J. Phys. Chem. B*, 2011, **115**, 2303–2311.
33 A. S. Thomas and A. H. Elcock, *J. Phys. Chem. Lett.*, 2011, **2**, 19–24.
34 B. J. Berne, J. D. Weeks and R. Zhou, *Annu. Rev. Phys. Chem.*, 2009, **60**, 85–103.
35 L. R. Pratt, M. I. Chaudhari and S. B. Rempe, *J. Phys. Chem. B*, 2016, **120**, 6455–6460.
36 D. Ben-Amotz, *J. Phys. Chem. Lett.*, 2015, **6**, 1696–1701.
37 D. Ben-Amotz, *Annu. Rev. Phys. Chem.*, 2016, **67**, 617–638.
38 A. Bartosik, M. Wiśniewska and M. Makowski, *J. Phys. Org. Chem.*, 2015, **28**, 10–16.
39 M. V. Athawale, S. N. Jamadagni and S. Garde, *J. Chem. Phys.*, 2009, **131**, 115102.
40 A. L. Ferguson, P. G. Debenedetti and A. Z. Panagiotopoulos, *J. Phys. Chem. B*, 2009, **113**, 6405–6414.
41 V. Hande and S. Chakrabarty, *ACS Omega*, 2022, **7**, 2671–2678.
42 I. Sinha, S. M. Cramer, H. S. Ashbaugh and S. Garde, *J. Phys. Chem. B*, 2022, **126**, 7604–7614.
43 P. Attard, *J. Chem. Phys.*, 1989, **91**, 3083–3089.
44 T. Biben, P. Bladon and D. Frenkel, *J. Phys.: Condens. Matter*, 1996, **8**, 10799.
45 R. Dickman, P. Attard and V. Simonian, *J. Chem. Phys.*, 1997, **107**, 205–213.
46 M. Dijkstra, R. van Roij and R. Evans, *Phys. Rev. E: Stat. Phys., Plasmas, Fluids, Relat. Interdiscip. Top.*, 1999, **59**, 5744.
47 R. Roth, R. Evans and S. Dietrich, *Phys. Rev. E: Stat. Phys., Plasmas, Fluids, Relat. Interdiscip. Top.*, 2000, **62**, 5360.
48 M. Kinoshita, *Chem. Phys. Lett.*, 2002, **353**, 259–269.
49 R. Akiyama, Y. Karino, Y. Hagiwara and M. Kinoshita, *J. Phys. Soc. Jpn.*, 2006, **75**, 064804.
50 T. Sumi and K. Koga, *Sci. Rep.*, 2019, **9**, 1–9.
51 T. Sumi and H. Imamura, *Protein Sci.*, 2021, **30**, 2132–2143.
52 J. L. F. Abascal and C. Vega, *J. Chem. Phys.*, 2005, **123**, 234505.
53 M. G. Martin and J. I. Siepmann, *J. Phys. Chem. B*, 1998, **102**, 2569–2577.
54 G. M. Torrie and J. P. Valleau, *Chem. Phys. Lett.*, 1974, **28**, 578–581.
55 G. M. Torrie and J. P. Valleau, *J. Comput. Phys.*, 1977, **23**, 187–199.
56 M. J. Abraham, T. Murtola, R. Schulz, S. Páll, J. C. Smith, B. Hess and E. Lindahl, *SoftwareX*, 2015, **1–2**, 19–25.
57 S. Kumar, D. Bouzida, R. H. Swendsen, P. A. Kollman and J. M. Rosenberg, *J. Comput. Chem.*, 1992, **13**, 1011–1021.
58 M. Souaille and B. Roux, *Comput. Phys. Commun.*, 2001, **135**, 40–57.
59 J. J. Nicolas, K. E. Gubbins, W. B. Streett and D. J. Tildesley, *Mol. Phys.*, 1979, **37**, 1429–1454.
60 Y. Kimura and Y. Yoshimura, *Mol. Phys.*, 1991, **72**, 279–294.
61 P. Krüger, S. K. Schnell, D. Bedeaux, S. Kjelstrup, T. J. Vlugt and J.-M. Simon, *J. Phys. Chem. Lett.*, 2013, **4**, 235–238.
62 N. Dawass, P. Krüger, S. K. Schnell, O. A. Moultos, I. G. Economou, T. J. Vlugt and J.-M. Simon, *Nanomaterials*, 2020, **10**, 771.

63 G. Graziano, *Chem. Phys. Lett.*, 2010, **499**, 79–82.
64 G. Graziano, *Chem. Phys. Lett.*, 2017, **685**, 54–59.
65 S. Asakura and F. Oosawa, *J. Chem. Phys.*, 1954, **22**, 1255–1256.
66 K. Koga, *J. Chem. Phys.*, 2002, **116**, 10882–10889.
67 K. Koga and H. Tanaka, *J. Chem. Phys.*, 2005, **122**, 104711.
68 B. Widom and R. C. Underwood, *J. Phys. Chem. B*, 2012, **116**, 9492–9499.
69 K. Koga, V. Holten and B. Widom, *J. Phys. Chem. B*, 2015, **119**, 13391–13397.
70 L. R. Pratt and D. Chandler, *J. Chem. Phys.*, 1980, **73**, 3434–3441.
71 K. Watanabe and H. C. Andersen, *J. Phys. Chem.*, 1986, **90**, 795–802.
72 D. Asthagiri, S. Merchant and L. R. Pratt, *J. Chem. Phys.*, 2008, **128**, 244512.
73 A. Gao, L. Tan, M. I. Chaudhari, D. Asthagiri, L. R. Pratt, S. B. Rempe and J. D. Weeks, *J. Phys. Chem. B*, 2018, **122**, 6272–6276.
74 T. Sumi and H. Sekino, *J. Chem. Phys.*, 2007, **126**, 04B614.
75 N. W. Lekkerkerker and R. Tuinier, *Colloids and the Depletion Interaction*, Springer, Heidelberg, 1st edn, 2011.
76 E. Y. Chi, S. Krishnan, T. W. Randolph and J. F. Carpenter, *Pharm. Res.*, 2003, **20**, 1325–1336.
77 S. Boeynaems, S. Alberti, N. L. Fawzi, T. Mittag, M. Polymenidou, F. Rousseau, J. Schymkowitz, J. Shorter, B. Wolozin, L. V. D. Bosch, P. Tompa and M. Fuxreiter, *Trends Cell Biol.*, 2018, **28**, 420–435.